Catalysis Communications 73 (2016) 1–6

Contents lists available at ScienceDirect

Catalysis Communications

journal homepage: www.elsevier.com/locate/catcom

Enhanced visible light photocatalytic activity and mechanism of $ZnSn(OH)_6$ nanocubes modified with AgI nanoparticles

Fei Chen, Qi Yang *, Chenggang Niu, Xiaoming Li, Chang Zhang, Jianwei Zhao, Qiuxiang Xu, Yu Zhong, Yaocheng Deng, Guangming Zeng

[a] College of Environmental Science and Engineering, Hunan University, Changsha 410082, P.R. China
[b] Key Laboratory of Environmental Biology and Pollution Control, Ministry of Education, Hunan University, Changsha 410082, P.R. China

ARTICLE INFO

Article history:
Received 5 August 2015
Received in revised form 12 September 2015
Accepted 1 October 2015
Available online 05 October 2015

Keywords:
Visible-light-driven
AgI/ZSH
Photocatalysis
RhB
Photodegradation mechanism

ABSTRACT

Novel visible-light-driven photocatalyst AgI/$ZnSn(OH)_6$ (AgI/ZSH) was synthesized by a facile deposition–precipitation method. The effect of several parameters such as the AgI loading, catalysts dosage and initial dye concentration on the photodegradation of rhodamine B (RhB) was investigated. The degradation efficiency of RhB could be almost 100% within 40 min and the removal rate of TOC reached 91% within 60 min at 20% AgI/ZSH dosage 1 g/L, which was 34 and 4.6 times of ZSH and AgI, respectively. The enhanced photoactivity of AgI/ZSH should be contributed to the faster separation of electron–hole pairs with ZSH as an electron trap.

1. Introduction

Nowadays, synthetic dyes that are widely used in textiles, printing, dyeing and food industries have been considered as one of major aquatic pollutants due to their toxicity, unpleasant coloring and non-biodegradability [1,2]. Moreover, most of the dyes and their degradation products may be carcinogenic and toxic to mammals [3,4]. Conventional chemical and biological treatment can remove dye from wastewater but seem to be not satisfied because of higher energy consumption and generation of toxic by-products [5,6]. Traditional physical techniques such as absorption, ultra-filtration and coagulation treatment may be more effective [7,8]. However they only realize the transfer of pollutants from water phase to another phase, thus causing the secondary pollution if no proper further treatment. In order to overcome these drawbacks, a new, eco-friendly and complete mineralization process for the dyes should be developed.

Photocatalysis technology has been widely investigated in the degradation of numerous organic/inorganic pollutants in recent years and is highly expected to be an ideal "green" pathway for environment purification and solar energy conversion [9–13]. In recent years, ZSH has become a new-type photocatalyst and is applied in photocatalytic degradation of organic pollutants, and due to its special structure full of OH groups, resulted in accepting photogenerated holes to form hydroxyl radical •OH [14–15]. For example, Fu et al. prepared ZSH by four methods [16], including grinding, co-precipitation, self-templating, and hydrothermal processes, to find out a suitable synthetic route for optimizing the photocatalytic performance of ZSH under a UV light. But ZSH had a wide-band energy of about 4.0 eV, limiting its application in the visible light area [17]. Some attempts had been concentrated in combining with other suitable band gap semiconductors for expanding the optical response range. Li and his co-workers had modified ZSH with BiOI, which exhibited high photoactivity in the degradation of dyes and phenol under both UV and visible light irradiation [18]. In our previous study, Ag/AgCl nanoparticles were introduced on the surface of ZSH composite to elevate the efficiency of electron–hole separation and to further achieve the highly efficient utilization of solar energy [19]. Modified ZSH had been demonstrated to be full of results, but the relative studies were still so few, it is urgent to find other adjustable semiconductors to improve the photocatalytic performance of ZSH under visible light.

Silver halides (AgX, X = Cl, Br, I) have been regarded as efficient photosensitive materials and source materials in the photography field. According to the previous researches, the AgX-based photocatalysts displayed excellent photocatalytic activity in the decomposition of organic pollutants [20–22]. As a member of AgX series, AgI possesses strong visible light absorption ability due to its narrow band gap (about 2.8 eV) [23]. In the Ag-based composites, the photoinduced electrons at the conduction band bottom of AgI could be transferred efficiently, which was favorable for the photocatalytic reaction. Considering the properties

---

* Corresponding author at: College of Environmental Science and Engineering, Hunan University, Changsha 410082, P.R. China.
E-mail addresses: feichen@hnu.edu.cn (F. Chen), Yangqi@hnu.edu.cn (Q. Yang).

http://dx.doi.org/10.1016/j.catcom.2015.10.003
1566-7367/

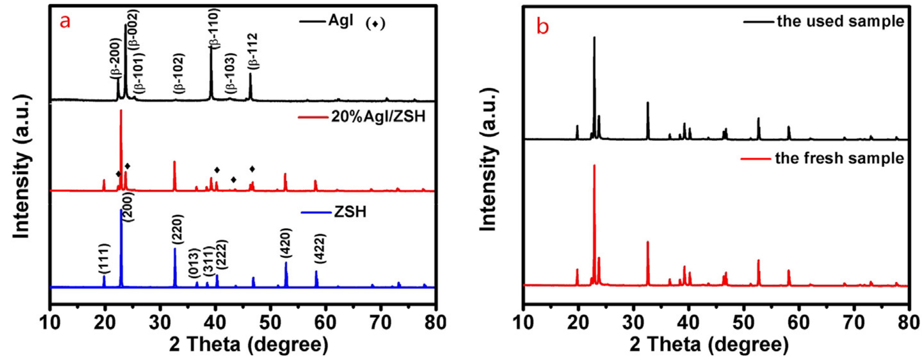

Fig. 1. XRD patterns of ZSH, AgI and 20% AgI/ZSH composite (a); and the fresh and used 20% AgI/ZSH composite (b).

of sensitizers, AgI could be used to modify the wide-band-gap semiconductors for enhancing the visible light absorption and utilization efficiency of solar energy, and the corresponding construction was listed as follows: AgI/TiO_2 [24,25], AgI/ZnO [26], AgI/$BiPO_4$ [27]. Nonetheless, there are still fewer investigations being performed on the composite photocatalysts containing AgI. Hence, the combination ZSH

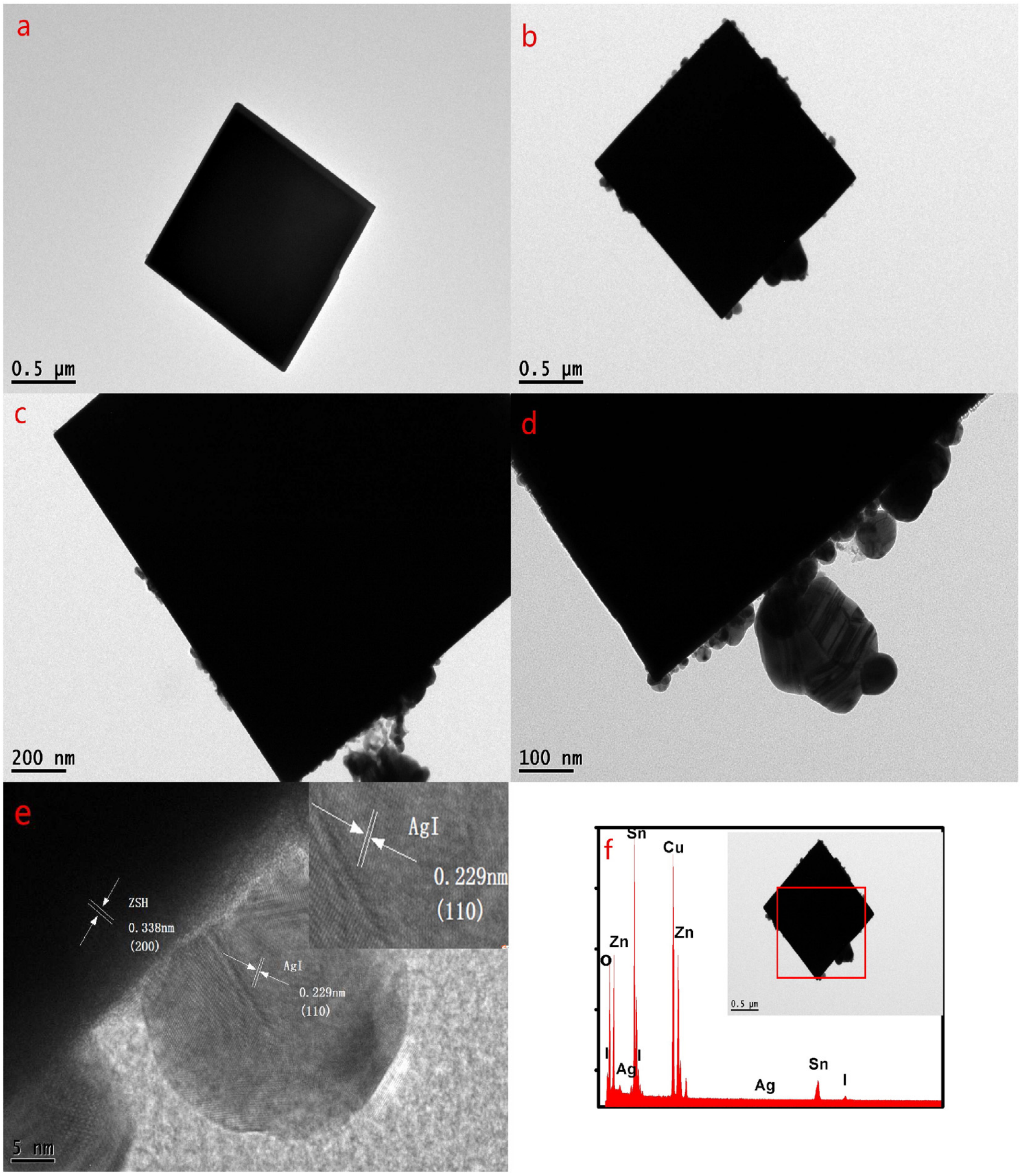

Fig. 2. TEM images of ZSH (a); 20% AgI/ZSH composite (b, c, d) and HRTEM image (e) and EDX (f) of 20% AgI/ZSH composite.

and AgI with suitable band potential by facile precipitation seems to be reasonable.

In this study, a novel AgI/ZSH composite was synthesized by deposition–precipitation method. The photoactivity of as-prepared samples was discussed by the photodecomposition of RhB in details. In addition, the recycling performance of the samples was evaluated for the long-term application. Through deep investigation of the structures and optical properties, the origin of excellent photocatalytic activity of AgI/ZSH composite was also explored.

2. Experimental

The whole experimental part was depicted in Supplementary information.

3. Result and discussion

3.1. Structure and morphology

The XRD patterns of ZSH, AgI and 20% AgI/ZSH composite were shown in Fig. 1a. It was clearly showed that the patterns of pure ZSH were consistent with the previous study [15], which could be indexed as cubic ZSH phase corresponding to JCPDS file NO. 73–2384. Furthermore, the diffraction peaks of AgI were identical to hexagonal β-AgI (JCPDS File No. 09–0374 [25]). The crystal planes of AgI in the AgI/ZSH curve were marked and the corresponding values were (200), (002), (110), (103) and (112). The other peaks in AgI/ZSH composite could be ascribed to the ZSH and no other impurities were found, indicating the high purity of the obtained photocatalysts. XRD patterns (Fig. 1b) of 20% AgI/ZSH composite before and after the photocatalytic reaction showed that the crystal structure remains constant, to further demonstrate that AgI/ZSH composite could be used as a potential photocatalyst for the organic pollutants removal.

The SEM analysis was presented in Supplementary information. The microstructure of 20% AgI/ZSH was further observed using TEM. From Fig. 2a, ZSH nanoboxes were observed clearly, while AgI nanoparticles were intimately attached to the surface and vicinity of ZSH (Fig. 2b, c, d in different magnifications). The interplanar spacing of the distinct lattice fringes is about 0.338 nm and 0.229 nm (Fig. 2e), which coincided with the plan of ZSH (200) and AgI (110), respectively. In addition, the EDX spectrum of the 20% AgI/ZSH composite revealed the coexistence of Zn, Sn, O, Ag and I (Fig. 2f). The weight ratio of AgI/ZSH was about 19.89%, which was in accordance with the preparation process.

3.2. XPS analysis

XPS was applied to characterize the surface information of the representative 20% AgI/ZSH composite. The peak position of the XPS spectra

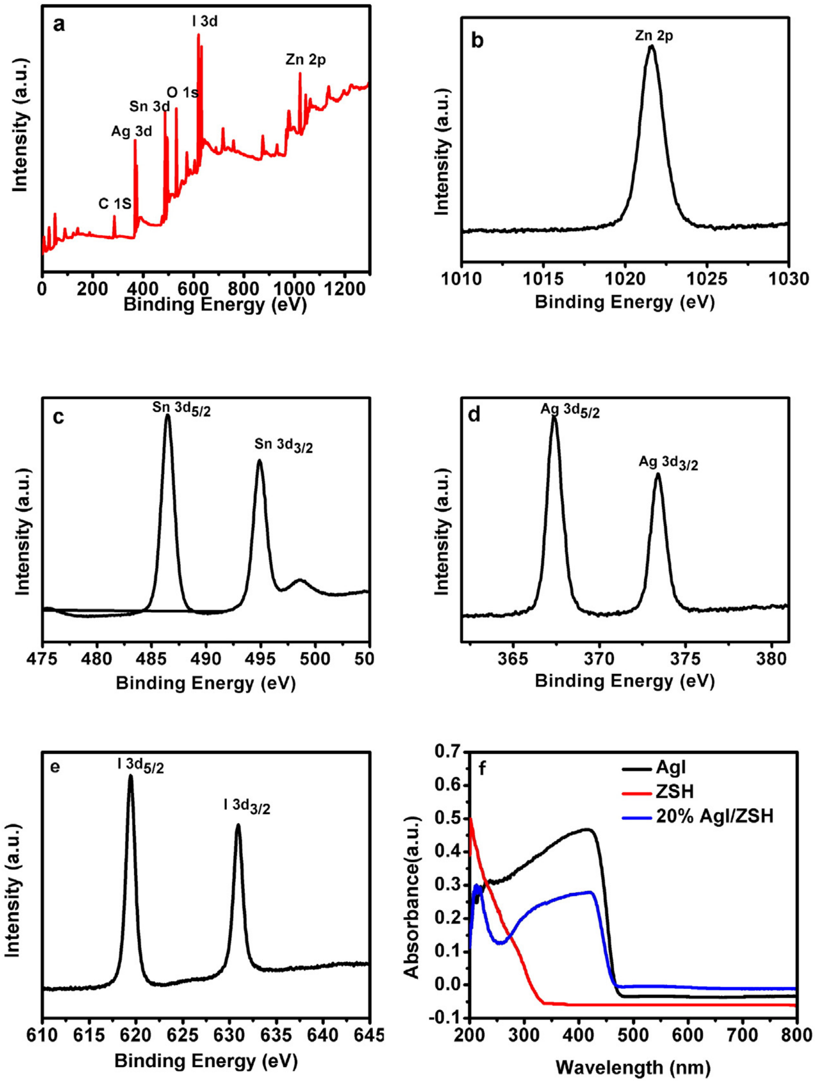

Fig. 3. XPS spectra (a–e) and DRS spectrum (f) of 20% AgI/ZSH composite.

was calibrated with C 1 s at 284.6 eV. Fig. 3a showed the survey XPS spectra of 20% AgI/ZSH composite. The result indicated that the synthesized product consists of Zn, Sn, O, Ag and I elements. The band energies of 1021.58 eV (Fig. 3b), 486.5 eV/495.1 eV (Fig. 3c) could be assigned to Zn 2p, Sn $3d_{5/2}$ and Sn $3d_{3/2}$, respectively, in accordance with the previous reports [17,18]. The peaks were detected at 373.7 eV and 367.7 eV (Fig. 3d) for Ag $3d_{3/2}$ and Ag $3d_{5/2}$, respectively, which could be ascribed to the band energies of Ag^+ in the fresh 20% AgI/ZSH composite [27]. From Fig. 3e, the I 3d XPS peaks could be resolved into two individual peaks 631.4 eV and 620.1 eV, corresponding to the band energies of I $3d_{3/2}$ and I $3d_{5/2}$, which was the characteristics of I^- in AgI [22]. The obtained results were in good agreement with the XRD analysis.

3.3. Optical properties

The optical properties of the AgI/ZSH samples were studied by the UV-spectroscopy. The pure ZSH only presented absorption in the UV light region about 334 nm (Fig. 3f), while pure AgI had a broader absorption at about 441 nm. The band gap of semiconductor photocatalysts could be estimated using the equation: $E_g = 1240/\lambda$ [28] (where λ is the absorption edge and E_g is the corresponding band gap). As depicted in Fig. 3f, the introduction of AgI nanoparticles, the absorption edge of the AgI/ZSH composite was extended to 330–450 nm (from UV to visible light region), verifying that absorption spectrum of ZSH was adjusted by the introduction of AgI nanoparticles.

3.4. Discussion of photocatalytic activities and stability

3.4.1. Effect of AgI loading amount and pseudo dynamics study

The photocatalytic activities of as-prepared AgI/ZSH composites were evaluated by the decomposition of the dye molecule RhB under visible light irradiation. As clearly shown in Fig. 4a, the RhB self-degradation and the dark absorption of RhB by the catalysts could be ignored. The photocatalytic activities of AgI/ZSH composites were highly enhanced and the removal efficiencies could achieve over 95%, while only 9.8% in the presence of ZSH. Fig. 4a showed that the optimal AgI loading was 20% weight ratio in AgI/ZSH composite, confirming that excessive AgI could lead to the recombination of photoinduced carriers. For comparison, N-TiO_2 and a physical mixture of AgI and ZSH (the weight ratio of AgI to ZSH was 20%) was also carried out for RhB degradation (Fig. 4b), whose photocatalytic activities were much weaker than 20% AgI/ZSH. The above results indicated that the heterostructure construction between AgI and ZSH played an important role in the enhancement of the visible light photoactivity, and the optimized amount of AgI in AgI/ZSH composite was 20%. Furthermore, the pseudo dynamic study was discussed in Supplementary information.

3.4.2. Effect of catalyst dosage and initial RhB concentration

Taken into consideration the economic condition, catalyst dosage is an important parameter in the constructed semiconductor photocatalysts [26,29]. As depicted in Fig. 4c, the effect of 20% AgI/ZSH composite dosage on the photodegradation of RhB was investigated in the range of 0.1 to 1.5 g/L. The photodegradation efficiencies of RhB firstly raised with the increase of dosage from 0.1 to 1.0 g/L, then decreased at 1.5 g/L, verifying that the moderate dosage of catalyst can lead more production of active species [30]. However, the suspension of excess catalyst dosage accumulated turbidity of solution, resulting in the reduction of the light penetration through the dye solution [31]. As displayed in Fig. 4d, initial RhB concentration was also an important factor and degradation efficiencies decreased with the increasing concentration (from 10 mg/L to 40 mg/L, 0.1 g of catalyst was added in RhB aqueous solution). This negative effect can be ascribed that a higher initial dye concentration decreases the path length of the photon entering the dye solution, resulting in lower photon adsorption on catalyst particles and consequently lowering the photocatalytic efficiency [32].

3.4.3. The mineralization ability of AgI/ZSH composite for RhB

Fig. 5a presented the mineralization ability of AgI/ZSH composite for the RhB in terms of TOC removal. In the photocatalytic system, the TOC removal was much slower than the degradation of RhB. After about

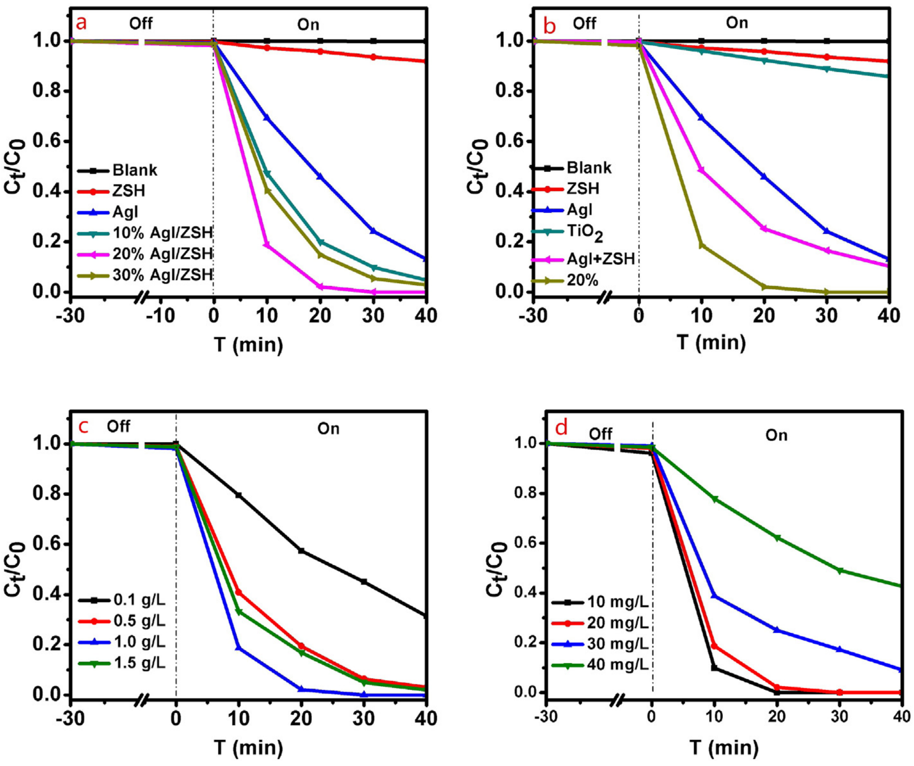

Fig. 4. Photodegradation of RhB of different weight ratios of AgI (a); Comparison of the degradation efficiencies by different samples (b); Effect of AgI/ZSH dosage (c) and initial RhB concentration (d) in the photodegradation process.

40 min, the removal efficiency of RhB reached 100% while the mineralization degree was only 79%. With the irradiation time extending to 60 min, the TOC removal improved to about 91%, confirming that no more by-products were generated in the degradation process. In addition, 20% AgI/ZSH composite maintained better photo-oxidation performance for RhB after four cycling runs (Fig. 5b), which suggested that the prepared photocatalyst possessed higher stability practical application.

4. Possible photocatalytic mechanism

To determine the main active species for the degradation of RhB solution in the photocatalytic process, three typical chemical reagents, Benzoquinone (BQ), Trietjanolamine (TEOA) and isopropanol (IPA), were adopted as the scavengers of •O^{2-}, h^+ and •OH, respectively [33–35]. It could be seen from Fig. 5c and Table 2 (Supplementary information) that the photodegradation of RhB was significantly suppressed by the addition of BQ and TEOA, while no reduction in the presence of IPA. The reaction rates changed from 0.237 min^{-1} (without scavengers) to 0.035 min^{-1}, 0.059 min^{-1} and 0.236 min^{-1} by the introduction of BQ, TEOA and IPA, respectively. These demonstrated that •O^{2-} and h^+ were the main active species in this photocatalytic process, which should be the synergetic effect of combined ZSH and AgI nanoparticles.

The generated main reactive species are described as following equations:

$$\mathrm{AgI} + h\gamma \rightarrow \mathrm{AgI}\ (h^+) + \mathrm{AgI}\ (e^-) \tag{1}$$

$$\mathrm{AgI}\ (e^-) + \mathrm{ZSH} \rightarrow \mathrm{AgI} + \mathrm{ZSH}\ (e^-) \tag{2}$$

$$\mathrm{ZSH}\ (e^-) + O_2 \rightarrow \mathrm{ZSH} + \bullet O^{2-} \tag{3}$$

$$\bullet O^{2-} + \text{organic pollutant} \rightarrow CO_2 + H_2O \tag{4}$$

$$h^+ + \text{organic pollutant} \rightarrow CO_2 + H_2O \tag{5}$$

On basis of the above experimental results, the possible degradation mechanism for AgI/ZSH composite was proposed and illustrated in

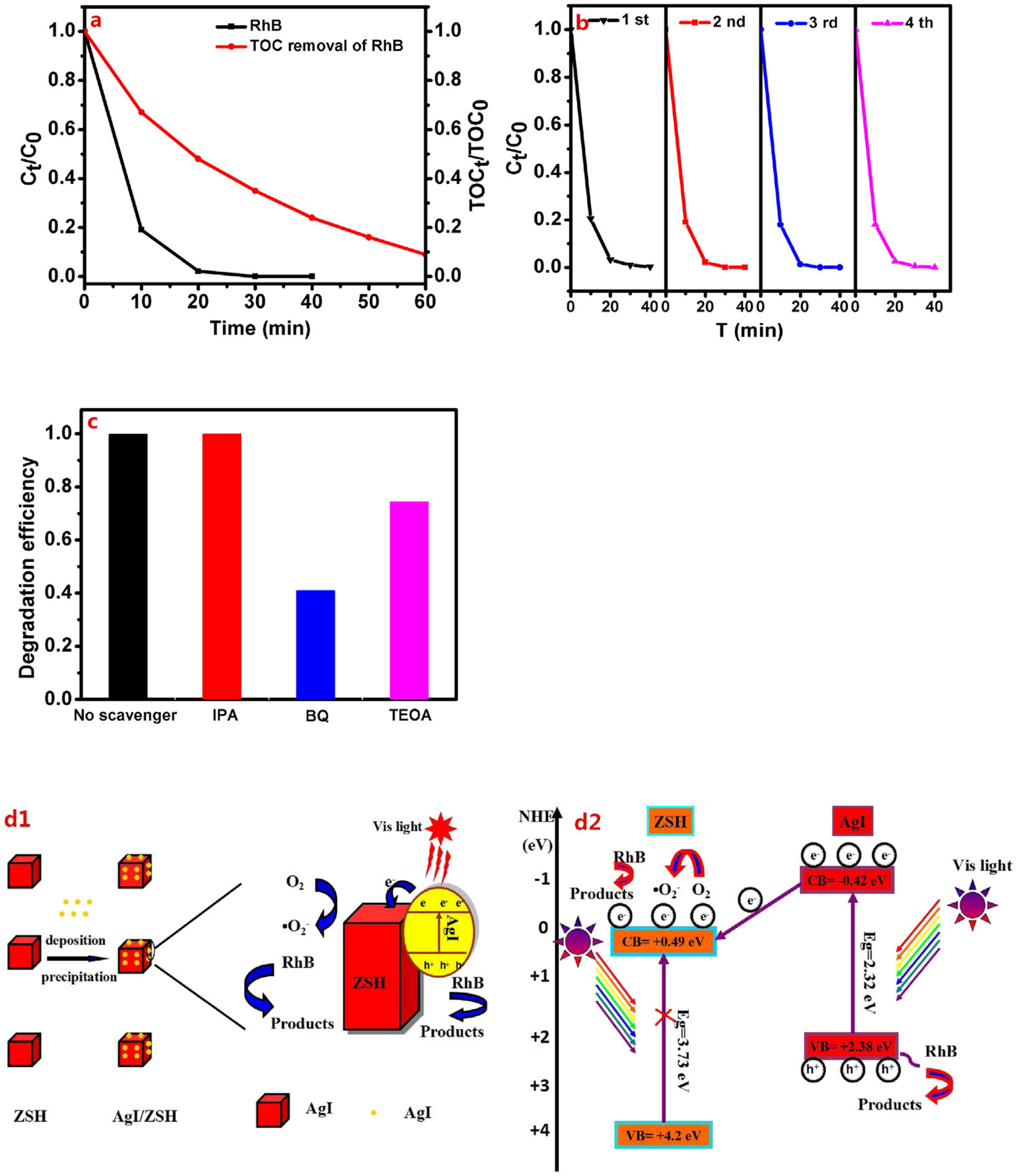

Fig. 5. TOC removal (a) cycling runs (b); photogenerated active species (c), the proposed mechanism (d) over RhB degradation by 20% AgI/ZSH composite.

Fig. 5d. According to the previous studies, the band gap energy of AgI and ZSH could be estimated as following empirical equations [26]:

$$E_{CB} = X - E_c - 0.5E_g \quad (6)$$

$$E_{VB} = E_{CB} + E_g \quad (7)$$

where X is the absolute electronegativity of the semiconductor, E_c is the energy of free electrons on the hydrogen scale (≈4.5 eV). Based on the band potential calculation, the E_{VB} of AgI and ZSH have been estimated to be +2.38 eV and +4.2 eV and the corresponding E_{CB} are −0.43 eV and +0.49 eV, respectively. Therefore, when the as-prepared catalyst was irradiated under visible light, only AgI could be excited to generalize electron–hole pairs and ZSH couldn't be excited due to its wide band gap. Because of the matching interactive energy band structure of AgI/ZSH composite, electrons generated in the CB of AgI (−0.43 eV) under visible light irradiation could migrate to the CB of ZSH (+0.49 eV), which was consistent with the previous reports [22,24]. The accumulated electrons could be trapped by dissolved oxygen to form $•O^{2-}$, which played an important role in photocatalytic degradation of RhB. Simultaneously, h^+ produced in the valence band of AgI could degrade dye directly. The vital role of ZSH in the forming AgI/ZSH composite was not only a good electron trap to efficiently separate the generated electron–holes by AgI, but also preventing the reduction process of Ag^+ to Ag^0 [27]. Through the internal mechanism, the constructed AgI/ZSH composite possessed better stability and exhibited highly enhanced photocatalytic activity in the degradation of organic pollutants under visible light irradiation.

5. Conclusions

Novel visible-light-driven AgI/ZSH photocatalyst was synthesized through introducing AgI nanoparticles on the ZSH with facile deposition–precipitation method. Among the as-prepared samples, 20% AgI/ZSH displayed the highest photocatalytic activity to the decomposition of RhB in aqueous solution under visible light irradiation. Compared with pure ZSH, AgI as well as N-doped TiO_2, AgI/ZSH possessed better mineralization ability for dye and was more stable. Mechanism study indicated that ZSH not only acted as an electron trap in the forming AgI/ZSH system to promote the separation of electron–hole pairs, but also ensured the stability of the catalyst. Our work may provide the insights to design more efficient and stable visible-light photocatalysts for textile wastewater treatment.

Acknowledgments

This research was financially supported by the project of National Natural Science Foundation of China (NSFC) (Nos. 51278175, 51378188, 51478170) and Doctoral Fund of Ministry of Education of China (20130161120021).

Appendix A. Supplementary data

Supplementary data to this article can be found online at http://dx.doi.org/10.1016/j.catcom.2015.10.003.

References

[1] A.A. Ahmad, B.H. Hameed, N. Aziz, J. Hazard. Mater. 141 (2007) 70–76.
[2] N. Barka, A. Assabbane, A. Nounah, Desalination 235 (2009) 264–275.
[3] Y.C. Hsiao, T.F. Wu, Y.S. Wang, C.C. Hu, C. Huang, Appl. Catal. B Environ. 148 (2014) 250–257.
[4] V. Vaiano, O. Sacco, D. Sannino, P. Ciambelli, Appl. Catal. B Environ. 170 (2015) 153–161.
[5] C.A. Martinez-Huitlea, E. Brillas, Appl. Catal. B Environ. 87 (2009) 105–145.
[6] A. Stolz, Appl. Microbiol. Biotechnol. 56 (2001) 69–80.
[7] C. Namasivayam, D. Kavitha, Dyes Pigments 54 (2002) 47–58.
[8] V.S. Mane, I.D. Mall, V.C. Srivastava, J. Environ. Manag. 84 (2007) 390–400.
[9] B.O. O'Regan, M. Gratzel, Nature 353 (1991) 737–740.
[10] M.R. Hoffmann, S.T. Martin, W. Choi, D.W. Bahnemann, Chem. Rev. 95 (1995) 69–96.
[11] M.S. Shah, A.R. Park, K. Zhang, J.H. Park, P.J. Yoo, ACS Appl. Mater. Interfaces 4 (2012) 3893–3901.
[12] X.B. Chen, S.H. Shen, L.J. Guo, S.L. Mao, Chem. Rev. 110 (2010) 6503–6570.
[13] T.S. Natarajan, M. Thomas, K. Natarajan, H.C. Bajaj, R.J. Tayade, Chem. Eng. J. 169 (2011) 126–134.
[14] Y.B. Chen, D.Z. Li, M. He, Y. Hu, H. Ruan, Appl. Catal. B Environ. 113 (2012) 134–140.
[15] Q. He, J.F. Zi, B.J. Huang, L.Y. Yan, W.J. Fa, J. Alloys Compd. 607 (2014) 193–197.
[16] X.L. Fu, D.W. Huang, Y. Qin, L.F. Li, Appl. Catal. B Environ. 148 (2014) 532–542.
[17] H.Q. Li, W.S. Hong, Y.M. Cui, Q.F. Jia, S.H. Fan, J. Mol. Catal. A Chem. 378 (2013) 164–173.
[18] H.Q. Li, Y.M. Cui, W.S. Hong, B.L. Xu, Chem. Eng. J. 228 (2013) 1110–1120.
[19] F. Chen, Q. Yang, C.G. Niu, X.M. Li, C. Zhang, G.M. Zeng, RSC Adv. 5 (2015) 63152–63164.
[20] J. Zhang, C.G. Niu, J. Ke, L.F. Zhou, G.M. Zeng, Catal. Commun. 59 (2015) 30–34.
[21] Y.P. Bi, S.X. Yang, J.Y. Cao, J.H. Ye, Phys. Chem. Chem. Phys. 13 (2011) 10071–10075.
[22] H. Xu, J. Yan, Y.G. Xu, Y.H. Song, H.M. Li, Appl. Catal. B Environ. 129 (2013) 182–193.
[23] W. Jiang, C.H. An, J.X. Liu, S.T. Wang, Dalton Trans. 43 (2014) 300–305.
[24] C. Hu, X.X. Hu, L.S. Wang, J.H. Qu, A.M. Wang, Environ. Sci. Technol. 40 (2006) 7903–7907.
[25] J.H. Yi, L.L. Huang, H.J. Wang, H. Yu, J. Hazard. Mater. 284 (2015) 207–214.
[26] X.J. Wang, X.L. Wan, X.N. Xu, X.N. Chen, Appl. Surf. Sci. 321 (2014) 10–18.
[27] H.F. Ye, H.L. Lin, J. Cao, S.F. Chen, J. Mol. Catal. A Chem. 397 (2015) 85–92.
[28] Z.Q. He, Y.Q. Shi, C. Gao, L. Wen, J. Phys. Chem. C 118 (2014) 389–398.
[29] M. Pirhashemi, A. Habibi-Yangjeh, J. Alloys Compd. 601 (2014) 1–8.
[30] M. Pelaez, N.T. Nolan, S.C. Pillai, Appl. Catal. B Environ. 125 (2012) 331–349.
[31] M. Rezaei, A. Habibi-Yangjeh, Appl. Surf. Sci. 265 (2013) 591–596.
[32] H. Wang, X.Z. Yuan, Y. Wu, G.M. Zeng, Appl. Catal. B Environ. 174 (2015) 445–454.
[33] L.H. Yu, W. Chen, D.Z. Li, J.B. Wang, Y. Shao, Appl. Catal. B Environ. 164 (2015) 453–461.
[34] J.C. Sun, Y.B. Zhang, J. Cheng, H. Fan, J. Mol. Catal. A Chem. 382 (2014) 146–153.
[35] X. Zhang, T. Guo, X. Wang, Y. Wang, C. Fan, H. Zhang, Appl. Catal. B Environ. 150 (2014) 486–495.